

Effect of Ni on Cu precipitation kinetics in α -Fe by AKMC study

Yi Wang,^{1,*} Huai Yu Hou,^{1,†} Xiang Bing Liu,² Rong Shan Wang,² and Jing Tao Wang^{1,‡}

¹*School of Materials Science and Engineering,*

Nanjing University of Science and Technology,

Nanjing 210094, People's Republic of China

²*Center of Plant Life Management,*

Suzhou Nuclear Power Research Institute, Suzhou 215004, China

Abstract

The kinetics of coherent Cu rich precipitation in Fe–Cu and Fe–Cu–Ni alloys during thermal ageing have been modeled by Atomic Kinetic Monte Carlo method (AKMC). The AKMC is parameterized by existing *ab-initio* data to treat vacancy mediated diffusion which is depend on local atomic environment. A nonlinear semi-empirical time adjusting method is proposed to rescaled the MC time. The combining AKMC and time adjusting method give a good agreement with experiments and other simulations, including advancement factor and the Cu cluster mobility. Simulations of ternary alloys reveal Ni has a temporal delay effect on Cu precipitation. This effect is caused by the decreasing of diffusion coefficient of Cu clusters. And the reduction effect of diffusion coefficient weakens with larger Cu cluster size. The simulation results can be used to explain the experimental phenomenon that ternary Fe–Cu–Ni alloys have higher cluster number density than corresponding binary alloy during coarsening stage, which is related to cluster mobility.

PACS numbers: 81.30.Mh, 66.30.-h, 64.75.Nx, 05.10.Ln

I. INTRODUCTION

Irradiation induced precipitation is believed to be one major reason for the degradation of mechanical properties of alloys in radiation environments. In α -Fe, which is the basis of ferritic steels, Cu rich precipitation from supersaturated matrix is greatly accelerated by irradiation. This kind of Cu rich precipitation is the primary reason of embrittlement for reactor pressure vessel (RPV) steels at low doses compared to the so called “late blooming phases” of MnNi rich precipitations¹ at high doses. Experiments show third-party elements such as Ni, Mn and Si etc. also exist in Cu rich precipitations and may have influence on Cu precipitation kinetics. In those elements, Ni and Mn are the richest elements in typical RPV steels². Possibly, they also have the strongest influence on Cu precipitation. Miller *et al.*^{3,4} found that a Fe-Cu-Mn model steel has the cluster density approximately an order of magnitude higher than that of Fe-Cu steel, and RPV steels with high nickel content may have retarded precipitation growth as evidenced by smaller cluster size. Meslin *et al.*⁵ discovered that advancement of precipitation is lower in the presence of Mn and Ni, suggesting they may delay the copper precipitation. The common summaries of experiments are higher precipitation number density or lower advancement is found in ternary alloys within same ageing time or radiation dose of binary alloy.

To further reveal the mechanism of the influence by third-party elements, atomic level computer simulation solutions seem to be attractive. Atomic kinetic Monte Carlo (AKMC) method based on diffusion of point defects has become an effective research tool on precipitation for having detailed information on atomic configuration in full time scale and being convenient to separate different factors. Vincent *et al.*⁶ studied the effect of Mn and Ni on Cu precipitation during radiation flux, the simulation results show Mn containing alloy has slightly smaller cluster size, while Ni seems to have little influence. Bonny *et al.*⁷ applied an artificial neural network (ANN) powered AKMC to study the precipitation of a ternary Fe-Cu-Ni alloy, and found the peak density of clusters increased by about 29% than binary alloy. However, due to the time evolution model used by previous works, the kinetics is not represented in view of real time evolution, e.g. MC time scale is found incomparable to experiments⁷, which limited further comparison.

In this study, we focus on the effect of Ni on Cu precipitation kinetics. To accomplish our aims, an AKMC approach is applied to simulate thermal ageing of Fe-Cu and Fe-Cu-Ni

alloys. The following content of this paper is divided into three parts. Detail of the computational methods used in the AKMC is presented in the first part. The parameterization is given and a nonlinear time adjusting method based on post-processing of AKMC data is proposed in order to reflect the kinetics correctly. In the second part, the simulation results are reported. Firstly, the simulation results of precipitation kinetics of the Fe–Cu binary system at varying temperatures are used to verify applicability of AKMC parameters and combined time adjusting method. Then the results of alloys with different Ni content, aged at same temperature, are compared. In the final part of the paper, the effect of Ni on Cu precipitation kinetics is discussed.

II. METHODS

In the AKMC simulation, the precipitation process is induced by thermal ageing. Initially, Cu and Ni substitutional atoms are randomly introduced into α -Fe matrix. A single vacancy is randomly introduced into the system to treat vacancy mediated diffusion.

A. AKMC simulation model

An AKMC code has been developed at Nanjing University of Science and Technology, with rigid on-lattice model (RLM) and Bortz–Kalos–Lebowitz (BKL) algorithm^{8,9}. When the vacancy lies on the first nearest neighbor lattice site of one atom, the probability of the position exchanging between this atom and the vacancy is obtained by the Arrhenius equation,

$$\Gamma_X = \nu_X \exp\left(-\frac{E_a}{k_B T}\right), \quad (1)$$

where ν_X is the attempt frequency for atom species X , which is related to local vibration modes¹⁰. In the present paper, ν_X values for all atom species are taken as one independent constant of $6 \times 10^{12} \text{ s}^{-1}$, which is on the same order of Debye frequency.

The time evolution of one KMC step is given by the summation of jump frequency of every possible exchanging,

$$\delta t = -\frac{\ln R}{\sum \Gamma_X}, \quad (2)$$

where, R is a uniform random number between 0 and 1.

B. Activation energy model

The activation energy in eq. (1) plays the key role in diffusion dynamics. Comprehensive description on energy models with heuristic formulas has been reported in Ref. 6, 11–13. Recently Vincent *et al.*¹⁴ made a critical review of these models. It is also possible to directly predict the activation energy by ANN AKMC^{15–17}. Here, we use the final initial system energy model (FISE)^{6,11,12}, which has the same form of the Kang–Weinberg decomposition¹⁸. For the situation of atom species X exchanging with a vacancy lying on the first nearest site, the activation energy writes as,

$$E_a \doteq \frac{E_{fnl} - E_{ini}}{2} + Q_X, \quad (3)$$

where E_{ini} and E_{fnl} are the initial and final system energies, respectively. Q_X is the migration energy of atom species X in α -Fe matrix.

The interaction of atoms is ranged up to second nearest neighbor and under two-body approximation, thus the system energy at a specific state is evaluated by summation of the energies of pairwise bonds, as following,

$$E = \sum_{i=1}^2 \sum_{j=1}^{Z_i} \varepsilon_{X-A_j}^{(i)} + \sum_{i=1}^2 \sum_{j=1}^{Z_i} \varepsilon_{V-B_j}^{(i)} - \varepsilon_{X-V}^{(1)}, \quad (4)$$

where i represents the bonds are counted in both first ($i=1$) and second ($i=2$) nearest neighbor sites. Z_i is the coordination number at each distance, A_j is a neighbor atom of the jumping atom X , B_j is a neighbor atom of the vacancy, ε is bond energy. X -V bond at first nearest neighbor distance is double counted, thus is subtracted in the third term.

Basic information on atom interactions is usually obtained by *ab-initio* calculations in a multi-scaled fashion. Results obtained by Vincent *et al.*^{6,19,20} has been opted in current study. The atomic interactions in Fe–Cu–Ni–Mn–Si system were studied using Projector Augmented-Wave (PAW) and UltraSoft Pseudo Potential (USPP) in their works. It was found that the USPP results reached a better agreement with experiments¹⁹. The values of Q_X for Fe, Cu and Ni are 0.62eV, 0.54eV and 0.68eV respectively¹⁹. In the present work, we fitted pairwise bond energies using a method similar to the description in Ref. 6. The *ab-initio* data of cohesive energy, mixing energy, binding energy and vacancy formation energy are expanded by following relations in RLM,

$$E_X^{coh} = 4\varepsilon_{X-X}^{(1)} + 3\varepsilon_{X-X}^{(2)}, \quad (5)$$

$$E_X^{sol}(\text{Fe}) = -4\varepsilon_{\text{Fe-Fe}}^{(1)} - 3\varepsilon_{\text{Fe-Fe}}^{(2)} + 8\varepsilon_{\text{Fe-X}}^{(1)} + 6\varepsilon_{\text{Fe-X}}^{(2)} - 4\varepsilon_{X-X}^{(1)} - 3\varepsilon_{X-X}^{(2)}, \quad (6)$$

$$E_{XY}^{b(i)}(\text{Fe}) = -\varepsilon_{\text{Fe-Fe}}^{(i)} + \varepsilon_{\text{Fe-X}}^{(i)} + \varepsilon_{\text{Fe-Y}}^{(i)} - \varepsilon_{X-Y}^{(i)}, \quad (7)$$

$$E_V^{for}(X) = 8\varepsilon_{X-V}^{(1)} + 6\varepsilon_{X-V}^{(2)} - 4\varepsilon_{X-X}^{(1)} - 3\varepsilon_{X-X}^{(2)}, \quad (8)$$

To balance the ratio between bond energies of X - Y pair on the first nearest and second nearest distance, extra equations are needed. Vincent *et al.*⁶ assumed a constant ratio between the second nearest bonds of X - X pair and Fe-Fe pair. Similarly, in Ref. 11, except the Cu-V bonds, the energy of a second nearest X - Y bond is half of the first nearest X - Y bond. Here we added extra equations by assuming the interfacial energies on $\{100\}$, $\{110\}$ and $\{111\}$ planes have negligible difference, as the following equations,

$$E_{XY}^{\text{int}\{110\}} = E_{XY}^{\text{int}\{100\}}, \quad (9)$$

$$E_{XY}^{\text{int}\{110\}} = E_{XY}^{\text{int}\{111\}}, \quad (10)$$

The interfacial energies can be expanded as equations,

$$E_{XY}^{\text{int}\{100\}} = -2\varepsilon_{X-X}^{(1)} - \varepsilon_{X-X}^{(2)} + 4\varepsilon_{X-Y}^{(1)} + 2\varepsilon_{X-Y}^{(2)} - 2\varepsilon_{Y-Y}^{(1)} - \varepsilon_{Y-Y}^{(2)}, \quad (11)$$

$$E_{XY}^{\text{int}\{110\}} = \left[-\varepsilon_{X-X}^{(1)} - \varepsilon_{X-X}^{(2)} + 2\varepsilon_{X-Y}^{(1)} + 2\varepsilon_{X-Y}^{(2)} - \varepsilon_{Y-Y}^{(1)} - \varepsilon_{Y-Y}^{(2)} \right] \cdot \sqrt{2}, \quad (12)$$

$$E_{XY}^{\text{int}\{111\}} = \left[-\frac{5}{2}\varepsilon_{X-X}^{(1)} - 3\varepsilon_{X-X}^{(2)} + 5\varepsilon_{X-Y}^{(1)} + 6\varepsilon_{X-Y}^{(2)} - \frac{5}{2}\varepsilon_{Y-Y}^{(1)} - 3\varepsilon_{Y-Y}^{(2)} \right] / \sqrt{3}, \quad (13)$$

Practically, our fitting is divided into two steps. In the first step, equations (5)(6)(7)(9)(10) are used to get the interactions between atoms. Then, in the second step, equations (7) and (8) are used to get the interactions between atoms and vacancy, where the interactions between atoms obtained by first step are considered to be known. In both steps, the equation sets are over-determined, the Moore Penrose generalized inverse matrix method was used to get the least square solution.

The fitted pairwise bond energies $\varepsilon_{X-Y}^{(i)}$ are given in Table I. It's worthwhile to notice that because the fitting equation sets are over-determined, not all equations are exactly equal on both sides at the end. Actually, only cohesive energies of Fe, Cu, Ni were exactly fitted, the values are -4.28eV, -3.49eV and -4.34eV respectively. Comparison of other energies is presented in Table II. The binding energies of Cu-Cu and Cu-V are obviously smaller than the *ab-initio* data. Though, mixing energy of Cu in α -Fe matrix was fitted well. We think it is because Cu- X pairs have strong many-body contribution that cannot be reproduced

TABLE I. Fitting result of pairwise bonds of atomic interactions

Bond $X-Y$	$\varepsilon_{X-Y}^{(i)}$ (eV)	
	$i=1$	$i=2$
Fe-Fe	-0.6856	-0.5125
Fe-Cu	-0.5696	-0.4429
Fe-Ni	-0.7099	-0.5201
Cu-Cu	-0.5610	-0.4153
Cu-Ni	-0.6600	-0.4764
Ni-Ni	-0.6903	-0.5263
Fe-V	-0.2117	-0.1035
Cu-V	-0.1853	-0.1611
Ni-V	-0.2601	-0.2767

by pairwise bonds. As is shown in Ref. 21, cluster expansion can get better fitting. It is also need to mention that for Cu and Ni, the reference structure for cohesive energies and mixing energies in Vincent's original work are fcc^{19,22}. Energy difference between fcc and bcc is 0.036eV for Cu by Domain and Becquart²³ and 0.10eV for Ni by Mishin *et al.*²⁴, though these small differences are ignored in fitting.

As suggested by Soisson and Fu¹¹, it seems necessary to introduce non-configurational entropy into the energy model to get better solubility of Cu, which is done by adding temperature dependent term for the Fe-Cu bond energies. We also used this method. Since saddle state is more related to initial state, this modification is only introduced into initial system energies. So E_{ini} becomes E'_{ini} with its pairwise bonds modified to $\varepsilon_{X-Y}^{(i)'} = \varepsilon_{X-Y}^{(i)} - \lambda_{X-Y}^{(i)}T$. The λ values for Fe-Cu pair are obtained by fitting Cu solubility in α -Fe, corresponding non-configurational entropy ΔS_{nc} equals $1.3k_B$, for Fe-Ni and X-V pairs, ΔS_{nc} were set as $1.0 k_B$. The λ factors for related pairs are listed in Table III.

C. Time adjusting

The time adjusting has special importance for AKMC thermal ageing simulations applied to solid solutions. For one reason the computation cost requires relatively smaller simula-

TABLE II. Comparison of target *ab-initio* thermodynamic properties and fitted results in RLM . Target values are from Ref. 19 (except the marked ones)

	target	fitted		target	fitted
E_{Cu}^{sol} (Fe)	0.55	0.5562	$E_{CuNi}^{b(1)}$ (Fe) ^b	0.065	0.0661
E_{Ni}^{sol} (Fe)	-0.17	-0.1804	$E_{CuNi}^{b(2)}$ (Fe) ^b	0.02	0.0258
$E_{CuCu}^{b(1)}$ (Fe)	0.16	0.1075	$E_{NiNi}^{b(1)}$ (Fe)	-0.10	-0.0440
$E_{CuCu}^{b(2)}$ (Fe)	0.05	0.0421	$E_{NiNi}^{b(2)}$ (Fe)	-0.02	-0.0015
E_V^{for} (Fe)	2.00	1.9658	$E_{CuV}^{b(1)}$ (Fe) ^c	0.16	0.0897
E_V^{for} (Cu) ^a	1.05	1.0412	$E_{CuV}^{b(2)}$ (Fe) ^c	0.18	0.1272
E_V^{for} (Ni)	0.60	0.5993	$E_{NiV}^{b(1)}$ (Fe)	0.03	0.0241
			$E_{NiV}^{b(2)}$ (Fe)	0.17	0.1656

^a The original value is 1.6eV, significantly higher than ab-initio result by Soisson *et al.*¹¹, also higher than prediction by interatomic potentials^{25–27}. So we modified it.

^b Fitting of original value gives incorrect number density, i.e. density decrease with increasing Ni content, so modified intentionally to a level according to the ternary potential of Bonny *et al.*²⁸.

^c Modified according to Ref. 23.

TABLE III. Entropy contribution factor λ for pairwise bonds

Bond $X-Y$	$\lambda_{X-Y}^{(i)}$	
	$i=1$	$i=2$
Fe-Cu	8.8450×10^{-6}	6.8774×10^{-6}
Fe-Ni	6.9518×10^{-6}	5.0930×10^{-6}
Fe-V	7.8816×10^{-6}	3.8534×10^{-6}
Cu-V	6.5202×10^{-6}	5.6686×10^{-6}
Ni-V	5.9914×10^{-6}	6.3738×10^{-6}

tion box which usually causing significant higher vacancy concentration and under-estimated time evolution. Moreover, phase separation progress results in evolving equilibrium vacancy concentration, while number of vacancies introduced in AKMC is fixed and integral. This difference cause time under-estimate degree evolves nonlinearly. We used the model described in Ref. 13, physical time is rescaled by the ratio between vacancy concentration

within matrix in MC model and equilibrium vacancy concentration of matrix,

$$dt_{\text{real}} = dt_{\text{MC}} \cdot \frac{C_V^{\text{MC}}(\text{M})}{C_V^{\text{eq}}(\text{M})}, \quad (14)$$

Equilibrium vacancy concentration of matrix is determined by vacancy formation energy in matrix, $C_V^{\text{eq}}(\text{M}) = \exp\left(\frac{\Delta S}{k_B}\right) \exp\left[-\frac{E_V^{\text{for}}(\text{M})}{k_B T}\right]$, ΔS is taken as $1.0 k_B$ as we mentioned above. Vacancy concentration within matrix in MC model is given by,

$$C_V^{\text{MC}}(\text{M}) = \frac{f_V^{\text{M}}}{N X_{\text{M}}}, \quad (15)$$

where, X_{M} is the concentration of matrix atoms(Fe) in the box, N is the total atom number. f_V^{M} is the ratio between equilibrium vacancy concentration in the solid solution and concentration in pure matrix.

Our concern focuses on the f_V^{M} value. There has not been a physical analysis for this value. In Ref. 11 and 13, it is regarded as fraction of time spent by the vacancy in Fe matrix, thus in their simulations the value was computed by checking if first and second nearest neighbors of vacancy contain Cu atom. One difficulty of this method is that because the system evolves nonlinearly with time, the ideal step length is nearly impossible to be obtained *on the fly*. As a consequence, the slope of $f_V^{\text{M}}(t)$ curve is slightly deviated at the beginning of simulation, and data fluctuation continuing become remarkable stronger with MC time increasing, especially in the coarsening stage. Here, we propose a semi-empirical way to get the f_V^{M} value. According to Lomer³¹, for a dilute solid solution, the value for ideal solution state can be determined physically, as well as the state when precipitation completed. Soisson and Fu¹¹ have given the expressions for Fe–Cu system,

$$f_V^{\text{M}}(0) = \frac{1 - z_1 C_{\text{Cu}} - z_2 C_{\text{Cu}}}{(1 - z_1 C_{\text{Cu}} - z_2 C_{\text{Cu}}) + \sum_{i=1}^2 z_i C_{\text{Cu}} \exp\left(\frac{E_{\text{CuV}}^{b(i)}(\text{Fe})}{k_B T}\right)}, \quad (16)$$

$$f_V^{\text{M}}(\infty) = 1 / \left[1 + \frac{C_{\text{Cu}}}{1 - C_{\text{Cu}}} \exp\left(\frac{E_V^{\text{for}}(\text{Fe}) - E_V^{\text{for}}(\text{Cu})}{k_B T}\right) \right], \quad (17)$$

The expressions give the upper and lower bounds for the f_V^{M} value. Since f_V^{M} decrease monotonically, an S-shape sigmoidal function is expected to link the bounds. The cluster number density, mean cluster size and advancement factor, also evolve with time, there should be a mapping relationship between the evolution of f_V^{M} and those quantities on the basis of time. Since the mentioned physical quantities can be calculated in post-processing,

if a sigmoidal function and mapping relationship of several special points is given, a semi-empirical function of f_V^M evolution can be obtained.

Since it is known evolution of advancement factor follows the Johnson–Mehl–Avrami (JMA) law, $\xi(t) = 1 - \exp[-(t/\tau)^n]$. f_V^M should evolve no slower than the order of JMA law. The sigmoidal Hill equation³² has been chosen to represent the f_V^M evolution, the formula is given as below,

$$\frac{\log(f) - \log(f_0)}{\log(f_\infty) - \log(f_0)} = \frac{1}{1 + (t_{\text{real}}/t_0)^p}, \quad (18)$$

where t_{real} is the real time, t_0 and p are unknown parameters.

Use a substitution $g = \log(t_{\text{real}})$, we get the following,

$$\frac{\log(f) - \log(f_0)}{\log(f_\infty) - \log(f_0)} = \frac{1}{1 + \exp[(g - g_0)/dx]}, \quad (19)$$

where $g_0 = \log(t_0)$ and $dx = 1/p$.

The expression on right of eq. (19) is known as Boltzmann equation. The $f_V^M(t)$ calculated in Ref. 11 got perfect fitting by this equation, with $g_0 \cong -0.82$ and $dx \cong 0.25$ (using 10 as the base of log function). This implies the eq. (19) has the correct “evolving speed”. So the next step to get the semi-empirical solution for f_V^M is to fit the unknown parameters of g_0 and dx .

We have chosen the number density of Cu clusters to give a mapping relationship of special points between post-processing data and f_V^M . The reason is that this variable does not evolve monotonically which making distinguish of different stages easily. On the number density evolution, two regions have the best analysis properties making them special. One is the time when nucleation starts, the other is the growth stage. When nucleation starts, binding of vacancy to clusters should has the most significant change, since random embryos from thermal fluctuation become stable nucleuses, this will cause a rapid change of the slope of the $f_V^M(t)$ curve. So we assumed the time nucleation starts, identified by when number density starts increasing, is mapped to the maximum curvature position ($\frac{d^4 f_V^M}{dt^4} = 0$) of $f_V^M(t)$ curve, that is $(g_0 + dx \cdot \ln(5 - 2\sqrt{6}), (3 + \sqrt{6})/6)$ for Boltzmann equation. Similarly, at growth stage, new nucleus stops to form, a maximum slope is expected since contribution to vacancy binding from nucleation is lost. We assumed the time growth starts mapped to the inflection point ($\frac{d^2 f_V^M}{dt^2} = 0$), that is $(g_0, 0.5)$, and identified by number density first reaches 90% of peak density. The mapping relationship is represented in Fig. 1. MC time

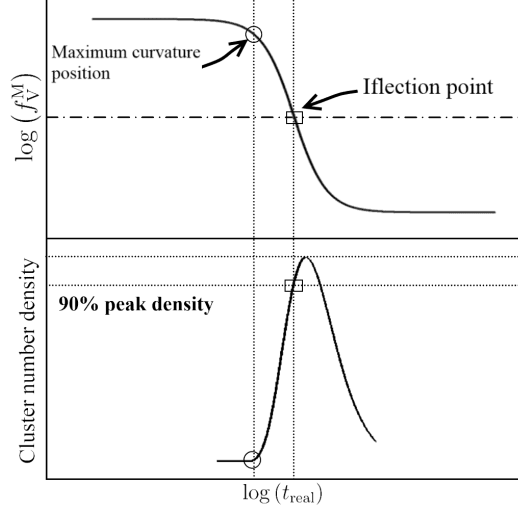


FIG. 1. Real time fitting scheme by relationship between number density and f_V^M .

of those two positions can be directly read from number density evolution, namely t_{MC}^n for time when nucleation starts and t_{MC}^g for time when growth starts. According to eq. (14), the MC time can be obtained by integration as a function of real time. Thus by solving the problem of equations (20) and (21) with proper optimization method, g_0 and dx can be fitted. Corresponding relationship between each MC time and real time can be obtained by numerical integration within an acceptable margin of error. This semi-empirical method is based on the post-processing of the number density data from AKMC and avoids complicate record step length setting and data fluctuation. The obtained $f_V^M(t)$ relationship is nonlinear as the vacancy bind energy evolution.

$$NX_M C_V^{eq}(M) \int_0^{nucleation-start} (1/f_V^M) dt_{real} = t_{MC}^n, \quad (20)$$

$$NX_M C_V^{eq}(M) \int_{nucleation-start}^{growth-start} (1/f_V^M) dt_{real} = t_{MC}^g - t_{MC}^n \quad (21)$$

III. RESULTS

A. Cluster identification

Cu rich clusters are identified by counting number of “bonds” linked to lattice sites. Those bonds are ranged up to second nearest neighbors as the activation energy model defined.

Since Fe atom is absent inside clusters in our results, which consist with other simulations, Fe atoms are ignored during the identification. Because of the time adjusting method we used, a lesser identify rule has been used, to be recognized as part of a cluster, one atom is required to be linked with at least three bonds. This geometrically causes the smallest cluster recognized is a tetrahedron.

B. Fe–Cu binary system kinetics

We applied the model above to simulate the precipitation kinetics of a Fe–1.34 at. % Cu alloy (about 1.4 wt. % Cu), during thermal ageing at four different temperatures, 663K, 713K, 773K and 873K respectively.

The advancement factor ξ , defined by eq. (22), represents the completeness of precipitation progress, and is a basic property which can be measured by several characteristics techniques.

$$\xi(t) = \frac{C_{\text{Cu}}(0) - C_{\text{Cu}}(t)}{C_{\text{Cu}}(0) - C_{\text{Cu}}(\infty)}, \quad (22)$$

in the equation, C_{Cu} is the concentration of solute Cu atoms. $C_{\text{Cu}}(0)$ is the initial Cu content, and $C_{\text{Cu}}(\infty)$ is the solubility of Cu in α -Fe which is estimated by the following equation,

$$C_{\text{Cu}}(\infty) \doteq \exp\left(\frac{\Delta S_{nc}^{\text{Cu}}}{k_B}\right) \exp\left[\frac{E_{\text{Cu}}^{\text{sol}}(\text{Fe})}{k_B T}\right], \quad (23)$$

where, $\Delta S_{nc}^{\text{Cu}}$ is the non-configurational entropy, and $E_{\text{Cu}}^{\text{sol}}(\text{Fe})$ is the mixing energy of Cu. To obtain the advancement factor, a simulation box containing $64 \times 64 \times 64$ bcc unit cells was used. The evolution of the advancement factor is shown in Fig. 2. The curves have good agreement with experiments overall the temperature range. Exceptions are, at low temperatures 663K and 713K, the kinetics are slower than experiment at the beginning of precipitation, and at high temperatures 773K and 873K, the kinetics are faster than experiments when $\xi > 0.6$. Even though, several simulation tests in bigger boxes ($128 \times 128 \times 128$) with ξ up to 0.7 show large box size seems to have better agreement. And, using more strict identification rule, i.e. cluster no smaller than 10 atoms, the kinetics will only be slightly slower at the beginning.

Advancement factor is still not enough to reflect all aspects of precipitation kinetics. A simulation box of $128 \times 128 \times 128$ unit cells has been used to get the number density and the

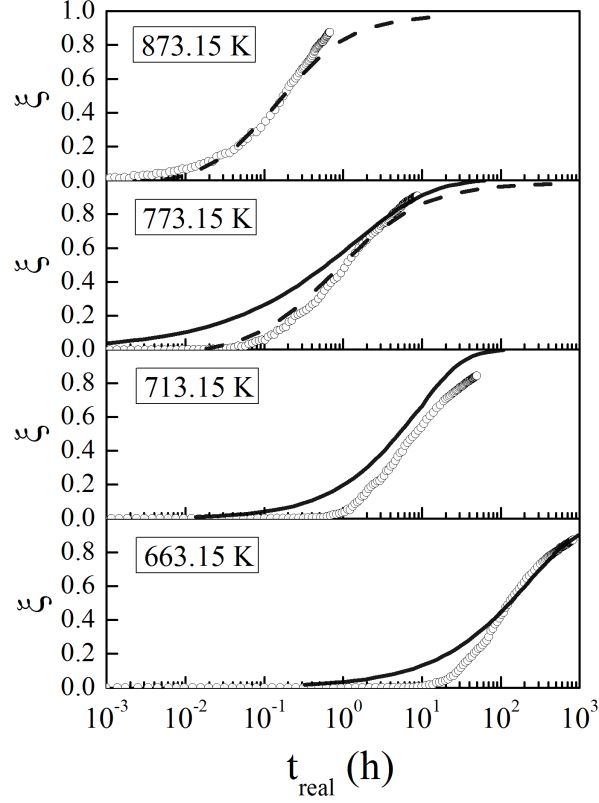


FIG. 2. Evolution of the advancement factor of Fe-1.34 at. % Cu under different temperatures.

mean cluster radius of Cu clusters. As is shown in Fig. 3(a), the number density and mean cluster size evolution has similar tendency of experiments. But the absolute value of the calculated number density is nearly a magnitude of order higher than the experiment data. In our AKMC result, after 10^0 h clusters are expected to have larger size than experiment detection limit, since the coarsening has already started. However, the number density after 10^0 h is still higher than experiments. So this kind of deviate is more than identification difference. To our knowledge, Castin *et al.*³³ gave the most satisfied result by hybrid AKMC method with ANN trained by an embedded atomic (EAM) potential²⁶. According to classical nucleation theory, the critical nucleation size is determined by volume free-energy change and interfacial energy of Cu cluster. The interfacial energies evaluated by our pairwise bonds are $E_{\text{FeCu}}^{\text{int}\{100\}}=0.5035\text{J/m}^2$, $E_{\text{FeCu}}^{\text{int}\{110\}}=0.4142\text{J/m}^2$ and $E_{\text{FeCu}}^{\text{int}\{111\}}=0.4465\text{J/m}^2$. And molecular statics calculation shows the EAM potential from Ref. 26 gives $E_{\text{FeCu}}^{\text{int}\{100\}}=0.3789\text{J/m}^2$, $E_{\text{FeCu}}^{\text{int}\{110\}}=0.4113\text{J/m}^2$ and $E_{\text{FeCu}}^{\text{int}\{111\}}=0.5130\text{J/m}^2$. The interfacial energies evaluated by both methods are close. However, as we mentioned before, the binding energies of Cu atoms are

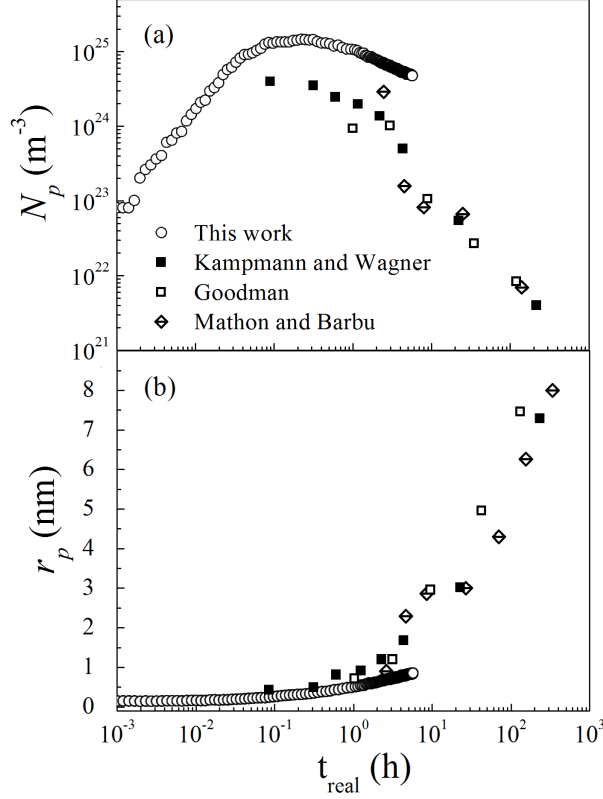


FIG. 3. Precipitation kinetics of Fe-1.34 at. % Cu under 773K, (a) cluster number density evolution $N_p(t)$, (b) mean cluster radius evolution $r_p(t)$. Experimental results are from Kampmann and Wagner: Ref. 34, Goodman: Ref. 35, Mathon and Barbu: Ref. 36 .

significantly under-estimated by pairwise bonds, the volume free-energy change should also be under-estimated. Thus the critical nucleation size will be under-estimated, result in a higher peak number density, as well as the density in coarsening stage.

It was first suggested by Soisson *et al.*^{11,37} that the Cu precipitation in α -Fe may favor a coagulation mechanism caused by highly mobile Cu clusters. This theory was recently confirmed by a hybrid AKMC method³³. We noticed that the difference between coagulation and emitting-absorbing mechanism only become marked in long term coarsening stage, our AKMC results seems to be not strong enough to be proved “correct”. It was mentioned that their Object KMC part is controlled by several parameters of Cu clusters, i.e. lifetime, diffusion coefficients and dissolution probability. Therefore we used the AKMC simulated mobility of VCu_N clusters at 773K. Fig. 4 shows the diffusion coefficients, lifetime and dissolution probability versus time, each data point was simulated for tens of thousands of times for statistics. The diffusion coefficients and lifetime have a good agreement with

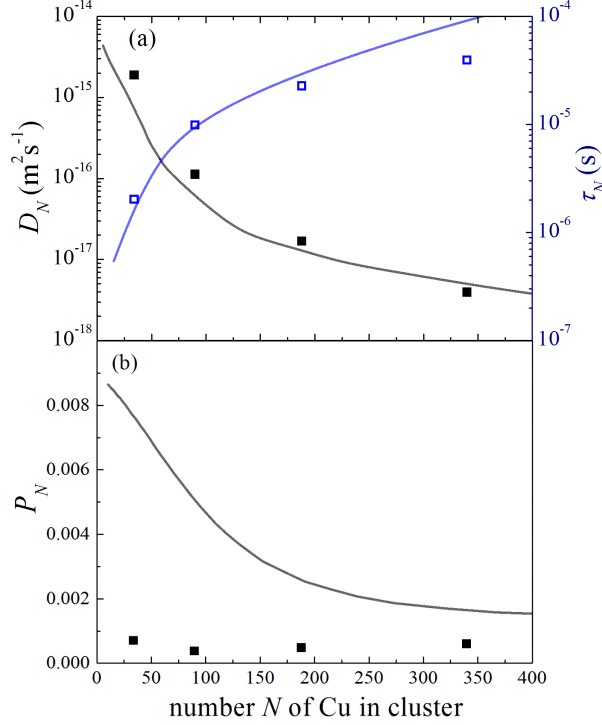


FIG. 4. Cluster mobility of VCu_N under 773K, (a) diffusion coefficients D_N and lifetime τ_N versus cluster number (b) dissolution probability P_N versus cluster number. Squares: this work; line: B-spline line of data from Ref.33.

Ref. 33. The dissolution probability by our model shows a different pattern, it does not decrease quickly with cluster size. However, the dissolution probability calculated by us is always lower than the probability in Ref. 33. It is apparent only a system with large dissolution probability will tend to emitting-absorbing mechanism. According to their work, even if dissolution is forbidden which means a dissolution probability of 0, the evolution still has good agreement with slight larger cluster size compared to experiments. So our model actually can reproduce the coagulation mechanism, rather than emitting-absorbing mechanism.

It has been shown from above results, our model reproduces consistent results with experiments and other simulations over a temperature range. The advancement factor was reproduced well, as well as the Cu cluster mobility. Although the cluster density is overestimated by our model, it is a drawback of pairwise bonds. Nevertheless, good description of Cu precipitation kinetics in binary Fe–Cu system has been obtained by our AKMC model and combined time adjusting method, the very first step needed for the study of Ni effect.

C. Fe–Cu–Ni ternary system kinetics

We performed thermal ageing simulations at 823K on Fe–1.34 at. % Cu – x at. % Ni alloys, the x values are 0, 0.5, 1.0, 1.5 and 2.0, respectively. The simulations were conducted in a box containing $128 \times 128 \times 128$ unit cells.

By direct visual observation from snapshot, we found that Ni appears to remain random distribution during the simulation, though some Ni atoms embellishes on Cu clusters like strawberry. Based on this fact, in the ternary alloys, one more rule was added to cluster identification, that is clusters should have only one pure Cu core no smaller than a tetrahedron. And, the bounds of f_V^M is extended as follows,

$$f_V^M(0) = \frac{\sum_{X=Cu, Ni} (1 - z_1 C_X - z_2 C_X)}{\sum_{X=Cu, Ni} \left[(1 - z_1 C_X - z_2 C_X) + \sum_{i=1}^2 z_i C_X \exp \left(\frac{E_{XV}^{b(i)}(\text{Fe})}{k_B T} \right) \right]}, \quad (24)$$

$$f_V^M(\infty) = \frac{1 - z_1 C_{Ni} - z_2 C_{Ni} - C_{Cu}}{\left(1 - C_{Cu} - \sum_{i=1}^2 z_i C_{Ni} \right) + C_{Cu} \exp \left(\frac{E_V^{for}(\text{Fe}) - E_V^{for}(\text{Cu})}{k_B T} \right) + \sum_{i=1}^2 z_i C_{Ni} \exp \left(\frac{E_{NiV}^{b(i)}(\text{Fe})}{k_B T} \right)}, \quad (25)$$

The advancement factor evolution is shown in Fig. 5(a). Starting from about $2 \times 10^{-2}h$, the precipitation kinetics become slower in four ternary alloys. When refer to Fig. 5(b) of number density evolution, we can see that, before number density reaches the peak number density the evolution of number density in ternary alloys is even slight faster. However, when passed the peak number density position, the evolution of number density in ternary alloys become obviously slower than the binary Fe–Cu alloy. The time $2 \times 10^{-2}h$ actually corresponds to the time at peak density. So from these observations it has been confirmed that the precipitation kinetics of ternary alloys appears to be “delayed” in the coarsening stage.

At the peak density point, the ternary alloys containing 1.5 at. % and 2.0 at. % Ni have about 10% higher number density than the binary alloy, while the other two ternary alloys are about 3% higher. It was found the peak number density of Cu clusters in Fe–1.13 at. % Cu–1.36 at. % Ni is about 29% higher than Fe–1.13 at. % Cu by ANN AKMC in Ref. 7. And the experimental results by Buswell *et al.*³⁸ gave about 34% higher peak number density by means of larger area under density-size distribution. Our result reproduced a similar tendency. The increasing peak number density is possibly caused by Ni effect on

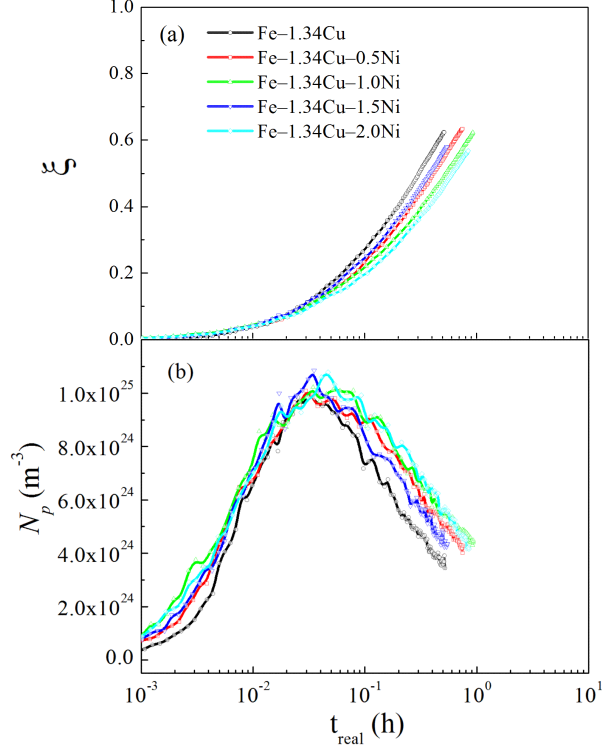


FIG. 5. Precipitation of Fe-Cu-Ni ternary alloys under 823K, (a) advancement factor evolution $\xi(t)$, (b) cluster number density evolution $N_p(t)$.

nucleation. Al-Motasem *et al.*³⁹ revealed Cu_mNi_n clusters have lower formation energy than pure Cu clusters. Seko *et al.*⁴⁰ also gave a similar result by *ab-initio* calculation. So the reason for a higher peak number density of Cu clusters is that Ni atoms act as nucleation centers for Cu precipitates and promote nucleation of Cu clusters. This also explains the more rapid evolution of ternary alloys during nucleation stage.

The mean surface area density of Ni atoms surrounding Cu cluster is shown in Fig. 6. The surface area density of Ni increases quickly with time and then saturates. The more Ni contains in a ternary alloy, the higher saturated surface area density of Ni is formed. Actually, a linear relationship has been found between the saturated surface area density of Ni and the Ni content of the alloy, with a slope around $1.46 \text{ nm}^{-2}/(1\%\text{Ni})$. The figure also confirmed visual observation that few Ni atoms embellish on Cu clusters, since the density is quite low.

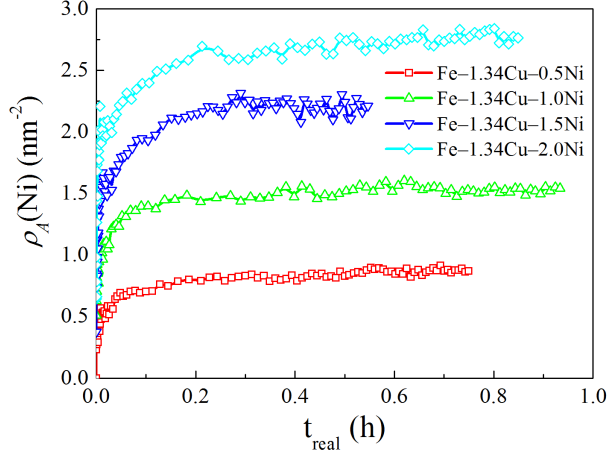


FIG. 6. The evolution of surface area density of Ni atoms on clusters $\rho_A(\text{Ni}) [t]$.

IV. DISCUSSION

One obvious effect of Ni on Cu precipitation is that higher cluster number density found in ternary alloys during coarsening stage compared to binary Fe–Cu alloy. In other alloy systems, similar phenomenon caused by third-party element atoms can also be found. For example, in Al–Sc–Zr alloys, addition of Zr is known to have an effect of producing higher density of $L1_2$ structure precipitation $\text{Al}_3\text{Sc}_x\text{Zr}_{1-x}$ during the coarsening stage^{41–43}. It will be interesting to compare the precipitation kinetics of these two alloys system. We plot the mean size evolution versus advancement factor of ternary Fe–Cu–Ni alloys in Fig. 7(a). As for Al–Sc–Zr system, the kinetic data are extracted from Ref. 44 and 45 within the time range from 0.3s to 0.5s, which seems comparable to our simulation time range. The cube root of mean size of precipitated $\text{Al}_3\text{Sc}_x\text{Zr}_{1-x}$ clusters versus total number of atoms in precipitations is represented in Fig. 7(b). The difference is quite remarkable, little change occurred by Ni addition. However, Zr addition significantly refines $\text{Al}_3\text{Sc}_x\text{Zr}_{1-x}$ precipitation. Clouet *et al.*⁴⁶ revealed that the diffusivity difference of Zr and Sc make Zr-rich external shell forming around the precipitation, which blocks Ostwald ripening. Based on the comparison from the figures, Ni plays a different role. The higher number density in Fe–Cu–Ni ternary alloys during coarsening stage is just because Ni somehow slows down the precipitation of Cu clusters. So Ni indeed has a temporal “delay” effect rather than refinement.

It is then natural to apply the cluster mobility analysis for the ternary alloys. We simulated the mobility of Cu clusters in Fe–Cu–Ni alloys at 823K. As is shown in Fig. 8, diffusion

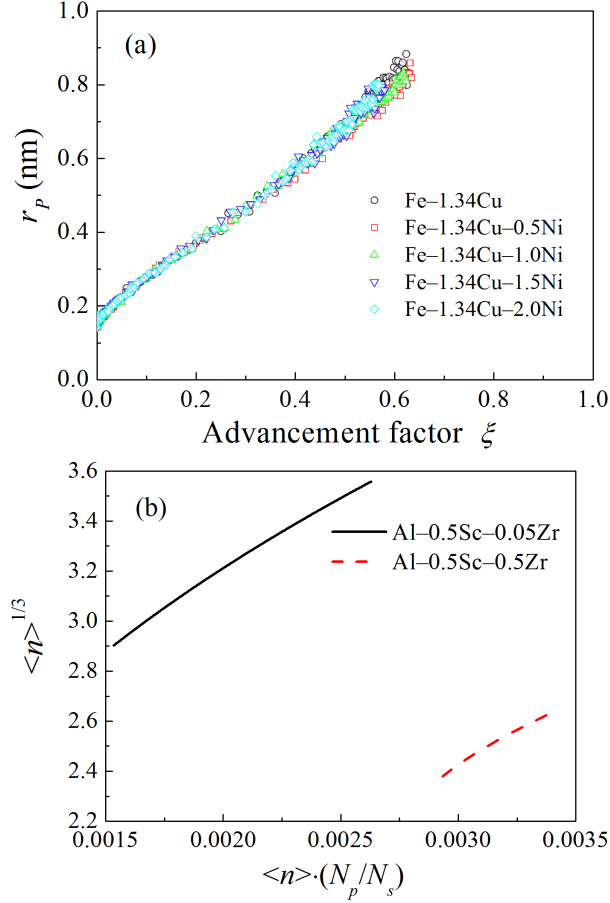


FIG. 7. Comparison of addition effect of third-party element on precipitation kinetics in view of mean size versus cluster density, (a) Ni effect in Fe-Cu-Ni alloys, (b) Zr effect in Al-Sc-Zr alloys.

coefficient decreases linearly with area density of Ni, a minimum of about 50% lower diffusion coefficient than binary alloy is found for studied area densities. While the life time of clusters increases with area density and has a maximum of about 25% higher than binary alloy for studied area densities. So the decreased diffusion coefficient is responsible for the delay effect of Ni. Even though, the slope of diffusion coefficient curves decreases with cluster size, larger clusters are less affected by the area density of Ni. So the delay effect by decreasing diffusion coefficient will be weakened with the clusters growing larger. Thus the Cu cluster number density of ternary alloys is expected to converge to a common value in the long term precipitation, which has been observed by experiments of Buswell *et al.*³⁸ and simulation of Bonny *et al.*⁷. Also, the linear law of decreasing diffusion coefficient may explain the sequence of the delayed curves of advancement factor and number density of ternary alloys. We actually have an unexpected sequence of 1.5 at. % -0.5 at. % -1.0 at.

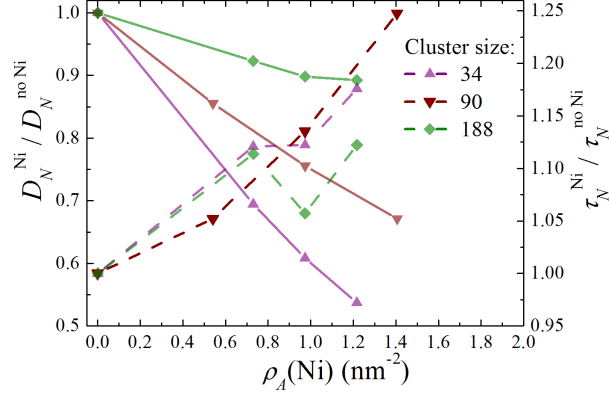


FIG. 8. Cluster mobility dependency of $\rho_A(\text{Ni})$ at 823K.

% -2.0 at. %, that is to say Fe-1.34 at. % Cu-1.5 at. % Ni is evolving faster than other ternary alloys in real time. While MC time gives an ordered 0.5 at. % -1.5 at. % -1.0 at. % -2.0 at. % sequence. Since f_V^M has a hyperbolic relationship with Ni content, and diffusion coefficient has a linear relationship, numerically they will yield a minimum time on a specific Ni content, which means a ternary alloy containin this Ni content has fastest evolution. It is possible that this specific Ni content is near 1.5 at. %.

V. CONCLUSION

We have simulated the precipitation during thermal ageing of binary Fe-Cu and ternary Fe-Cu-Ni alloys by AKMC method. The energy model is based on a two-body short range model. A nonlinear time adjusting method from post-processing data has been proposed. Using the combined computational techniques, though the cluster density is over-estimated, good agreement of Cu precipitation kinetics has been obtained over a temperature range. For the effect of Ni on Cu precipitation, the following conclusions have been found:

1. Peak number density of Cu clusters is higher in Fe-Cu-Ni ternary alloys, which can be explained by Ni promoting nucleation of Cu clusters. Surface area density of Ni on clusters has a linear relationship with Ni content;
2. A delay effect has been found for Ni on Cu precipitation in the coarsening stage. Comparison with Al-Sc-Zr alloys reveals this effect is mainly temporal, rather than refinement of precipitations;

3. Diffusion coefficient decreases linearly with area density of Ni, while life time increases. This Decreasing effect of the cluster diffusion coefficient is responsible for the delay effect. Even though, this effect weakens with larger cluster size.

On the other side, limitation of this AKMC study still remains. We are working on better activation energy model to over-come the shortcoming of pairwise energy model.

ACKNOWLEDGMENTS

This work is funded by the National Natural Science Foundation of China under grants 51071111 and by the the National High Technology Research and Development Program of China (863 Program) under grants 2012AA050901. The authors would like to thank the support by Suzhou Nuclear Power Research Institute.

ï»¿

* yiwang_cn@126.com

† hyhou@njust.edu.cn

‡ jtwang@njust.edu.cn

¹ G. R. Odette, MRS Proceedings **373** (1994), 10.1557/PROC-373-137.

² “Standard specification for quenched and tempered vacuum-treated carbon and alloy steel forgings for pressure vessels,” (2005).

³ M. Miller, B. Wirth, and G. Odette, Materials Science and Engineering: A **353**, 133 (2003), <ce:title>47 th International Field Emission Symposium</ce:title>.

⁴ M. Miller, M. Sokolov, R. Nanstad, and K. Russell, Journal of Nuclear Materials **351**, 187 (2006), <ce:title>Proceedings of the Symposium on Microstructural Processes in Irradiated Materials</ce:title> <xocs:full-name>Proceedings of the Symposium on Microstructural Processes in Irradiated Materials</xocs:full-name>.

⁵ E. Meslin, B. Radiguet, P. Pareige, and A. Barbu, Journal of Nuclear Materials **399**, 137 (2010).

⁶ E. Vincent, C. Becquart, and C. Domain, Journal of Nuclear Materials **382**, 154 (2008), <ce:title>Microstructural Processes in Irradiated Materials</ce:title> <xocs:full-

- name>Proceedings of the Symposium on Microstructural Processes in Irradiated Materials, as part of the annual meeting of The Minerals, Metals & Materials Society</xocs:full-name>.
- ⁷ G. Bonny, R. Pasianot, N. Castin, and L. Malerba, Philosophical Magazine **89**, 3531 (2009), <http://www.tandfonline.com/doi/pdf/10.1080/14786430903299824>.
 - ⁸ J. Marro, A. B. Bortz, M. H. Kalos, and J. L. Lebowitz, Phys. Rev. B **12**, 2000 (1975).
 - ⁹ A. Bortz, M. Kalos, and J. Lebowitz, Journal of Computational Physics **17**, 10 (1975).
 - ¹⁰ G. H. Vineyard, Journal of Physics and Chemistry of Solids **3**, 121 (1957).
 - ¹¹ F. Soisson and C.-C. Fu, Phys. Rev. B **76**, 214102 (2007).
 - ¹² C. S. Becquart and C. Domain, physica status solidi (b) **247**, 9 (2010).
 - ¹³ Y. L. Bouar and F. Soisson, Phys. Rev. B **65**, 094103 (2002).
 - ¹⁴ E. Vincent, C. Becquart, C. Pareige, P. Pareige, and C. Domain, Journal of Nuclear Materials **373**, 387 (2008).
 - ¹⁵ F. Djurabekova, R. Domingos, G. Cerchiara, N. Castin, E. Vincent, and L. Malerba, Nuclear Instruments and Methods in Physics Research Section B: Beam Interactions with Materials and Atom
`<ce:title>Computer Simulation of Radiation Effects in Solids</ce:title>`
`<ce:subtitle>Proceedings of the Eighth International Conference on Computer Simula-`
`tion of Radiation Effects in Solids (COSIRES 2006)</ce:subtitle>` `<xocs:full-name>Computer`
`Simulation of Radiation Effects in Solids</xocs:full-name>.`
 - ¹⁶ N. Castin and L. Malerba, The Journal of Chemical Physics **132**, 074507 (2010).
 - ¹⁷ N. Castin, L. Malerba, G. Bonny, M. Pascuet, and M. Hou, Nuclear Instruments and Methods in Physics Research Section B: Beam Interactions with Materials and Atom
`<ce:title>Proceedings of the Ninth International Conference on Computer Simulation of Radi-`
`ation Effects in Solids</ce:title>.`
 - ¹⁸ H. C. Kang and W. H. Weinberg, The Journal of Chemical Physics **90**, 2824 (1989).
 - ¹⁹ E. Vincent, *Simulations numériques à l'échelle atomique de l'évolution microstructura*, Ph.D. thesis, Université Lille I (2008).
 - ²⁰ E. Vincent, C. Becquart, and C. Domain, Nuclear Instruments and Methods in Physics Research Section B: Be
`<ce:title>Proceedings of the Seventh International Conference on Computer Simulation of`
`Radiation Effects in Solids</ce:title>.`
 - ²¹ F. Soisson and C. C. Fu, Solid State Phenomena **129**, 31 (2007).

- ²² E. Vincent, C. Becquart, and C. Domain, Journal of Nuclear Materials **351**, 88 (2006),
<ce:title>Proceedings of the Symposium on Microstructural Processes in Irradiated Materi-
als</ce:title> <xocs:full-name>Proceedings of the Symposium on Microstructural Processes in
Irradiated Materials</xocs:full-name>.
- ²³ C. Domain and C. S. Becquart, Phys. Rev. B **65**, 024103 (2001).
- ²⁴ Y. Mishin, M. Mehl, and D. Papaconstantopoulos, Acta Materialia **53**, 4029 (2005).
- ²⁵ G. J. Ackland, D. J. Bacon, A. F. Calder, and T. Harry,
Philosophical Magazine A **75**, 713 (1997), <http://www.tandfonline.com/doi/pdf/10.1080/01418619708207198>.
- ²⁶ R. Pasianot and L. Malerba, Journal of Nuclear Materials **360**, 118 (2007).
- ²⁷ H. Huai Yu, W. Rong Shan, W. Jing Tao, L. Xiang Bing, C. Guang, and H. Ping,
Modelling and Simulation in Materials Science and Engineering **20**, 045016 (2012).
- ²⁸ G. Bonny, R. Pasianot, and L. Malerba, Philosophical Magazine **89**, 3451 (2009),
<http://www.tandfonline.com/doi/pdf/10.1080/14786430903299337>.
- ²⁹ S. Miloudi, *Etude du dommage d'irradiation dans les aciers de cuve des réacteurs à eau pres-*
surisée, Ph.D. thesis, Université de Paris-Sud (1997).
- ³⁰ G. Salje and M. Feller-Kniepmeier, Journal of Applied Physics **48**, 1833 (1977).
- ³¹ W. M. Lomer, "Vacancies and other point defects in metals and alloys," (Institute of Metals,
London, 1958) Chap. Point Defects and Diffusion in Metals and Alloys, p. 79.
- ³² A. V. Hill, The Journal of Physiology **40(Suppl)**, iv (1910).
- ³³ N. Castin, M. I. Pascuet, and L. Malerba, The Journal of Chemical Physics **135**, 064502 (2011).
- ³⁴ R. Kampmann and R. Wagner, in *Atomic Transport and Defects in Metals by Neutron Scattering*,
Springer Proceedings in Physics, Vol. 10, edited by C. Janot, W. Petry, D. Richter, and
T. Springer (Springer Berlin Heidelberg, 1986) pp. 73–77.
- ³⁵ S. Goodman, S. Brenner, and J. Low, Metallurgical Transactions **4**, 2371 (1973).
- ³⁶ M. Mathon, A. Barbu, F. Dunstetter, F. Maury, N. Lorenzelli, and C. de Novion,
Journal of Nuclear Materials **245**, 224 (1997).
- ³⁷ F. Soisson, A. Barbu, and G. Martin, Acta Materialia **44**, 3789 (1996).
- ³⁸ J. T. Buswell, C. A. English, M. G. Hetherington, W. J. Phythian, W. Smith, and G. M.
Worrall, in *Effects of Radiation on Materials: 14th International Symposium, ASTM STP 1046*,
II, Vol. 127, edited by N. H. Packan, R. E. Stoller, and A. S. Kumar (ASME, Philadelphia,
1990).

- ³⁹ A. Al-Motasem, M. Posselt, and F. Bergner, *Journal of Nuclear Materials* **418**, 215 (2011).
- ⁴⁰ A. SEKO, N. ODAGAKI, S. R. NISHITANI, T. I., and A. H., *Materials Transactions* **45**, 1978 (2004).
- ⁴¹ A. Deschamps, L. Lae, and P. Guyot, *Acta Materialia* **55**, 2775 (2007).
- ⁴² C. B. Fuller, J. L. Murray, and D. N. Seidman, *Acta Materialia* **53**, 5401 (2005).
- ⁴³ C. B. Fuller and D. N. Seidman, *Acta Materialia* **53**, 5415 (2005).
- ⁴⁴ E. Clouet, M. Nastar, A. Barbu, C. Sigli, and G. Martin, *Advanced Engineering Materials* **8**, 1228 (2006).
- ⁴⁵ E. Clouet, M. Nastar, A. Barbu, C. Sigli, and G. Martin, in *Solid-Solid Phase Transformations in Inorganic Materials*, Vol. 2, edited by J. M. Howe, D. E. Laughlin, J. K. Lee, U. Dahmen, and W. A. Soffa (TMS, 2005) Chap. Precipitation in Al-Zr-Sc alloys: a comparison between kinetic Monte Carlo, cluster dynamics and classical nucleation theory, pp. 683–703.
- ⁴⁶ E. Clouet, L. Lae, T. Epicier, W. Lefebvre, M. Nastar, and A. Deschamps, *Nat Mater* **5**, 482 (2006).